

NRL FR-7734

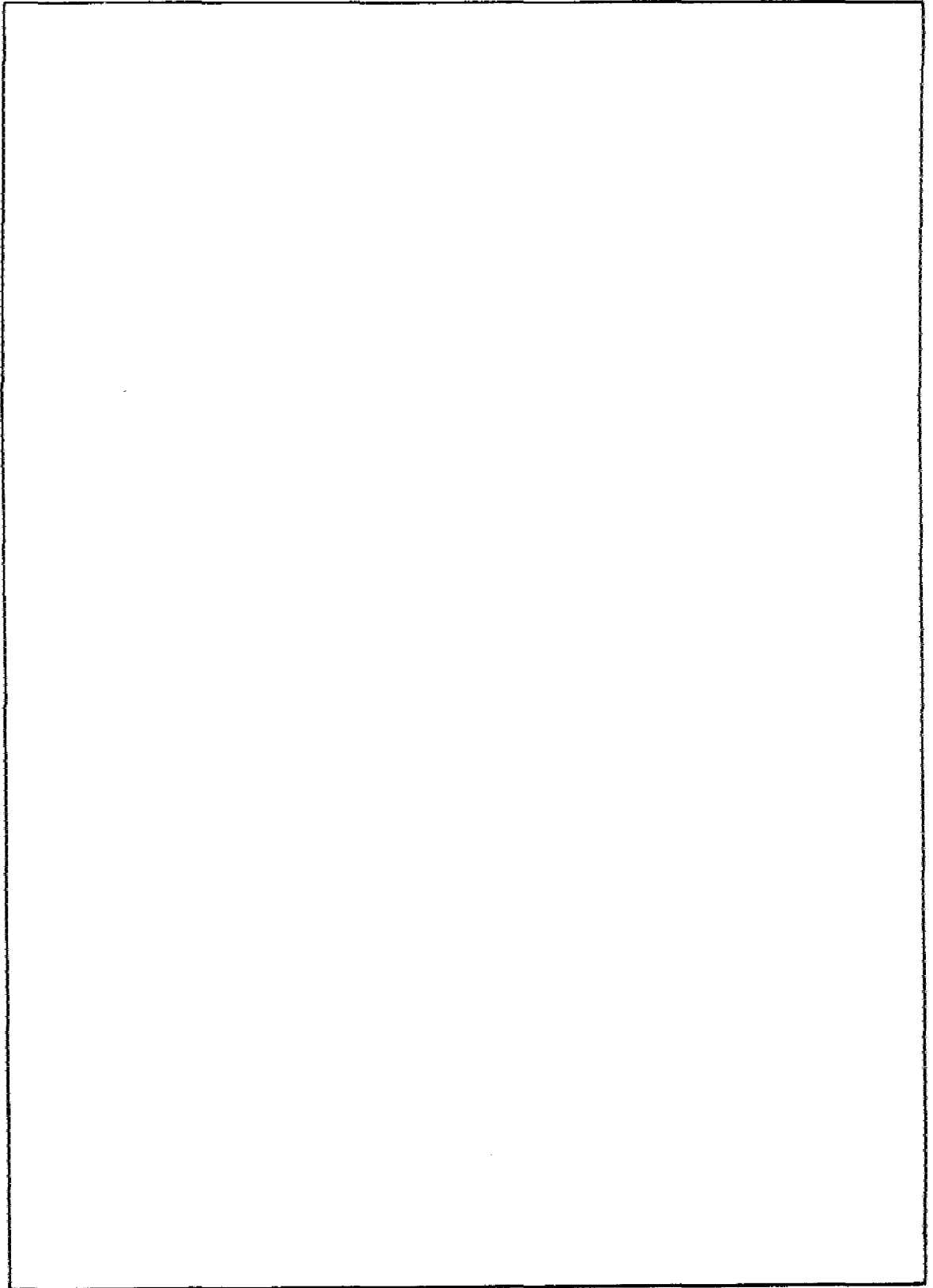
A Detector Design for the SPS-10 Radar

B.H. Cantrell  
G.V. Trunk  
P.D. Queen

June 19, 1974

Naval Research Laboratory  
Washington D.C. 20362

REPORT DOCUMENTATION PAGE		READ INSTRUCTIONS BEFORE COMPLETING FORM
1. REPORT NUMBER NRL Report 7734	2. GOVT ACCESSION NO.	3. RECIPIENT'S CATALOG NUMBER
4. TITLE (and Subtitle) A DETECTOR DESIGN FOR THE SPS-10 RADAR	5. TYPE OF REPORT & PERIOD COVERED Interim Report	
	6. PERFORMING ORG. REPORT NUMBER	
7. AUTHOR(s) B. H. Cantrell, G. V. Trunk, F. D. Queen	8. CONTRACT OR GRANT NUMBER(s)	
9. PERFORMING ORGANIZATION NAME AND ADDRESS Naval Research Laboratory Washington, D.C. 20375	10. PROGRAM ELEMENT PROJECT, TASK AREA & WORK UNIT NUMBERS NRL Problem R02-54 RF 12-151-403-4010	
11. CONTROLLING OFFICE NAME AND ADDRESS Department of the Navy Office of Naval Research Arlington, Va. 22217	12. REPORT DATE June 19, 1974	
	13. NUMBER OF PAGES 22	
14. MONITORING AGENCY NAME & ADDRESS (if different from Controlling Office)	15. SECURITY CLASS. (of this report) Unclassified	
	15a. DECLASSIFICATION/DOWNGRADING SCHEDULE	
16. DISTRIBUTION STATEMENT (of this Report) Approved for public release; distribution unlimited.		
17. DISTRIBUTION STATEMENT (of the abstract entered in Block 20, if different from Report)		
18. SUPPLEMENTARY NOTES		
19. KEY WORDS (Continue on reverse side if necessary and identify by block number) Radar detection Video integration Thresholding		
20. ABSTRACT (Continue on reverse side if necessary and identify by block number) An automatic detector to be used with the SPS-10 radar was designed. The parametric detector consists of a 2-pole video integrator and uses an adaptive threshold. The threshold is set by obtaining an estimate of the mean and variance from the surrounding region (range and azimuth) of the sample under test. The operating characteristics of the detector are presented for both thermal noise and clutter conditions.		



## CONTENTS

INTRODUCTION .....	1
DETECTOR SELECTION .....	1
Nonparametric Detectors .....	1
Parametric Detectors .....	2
DETECTOR IMPLEMENTATION .....	2
Analog-to-Digital Converter .....	2
Two-Pole Filter .....	3
Estimates of Mean and Standard Deviation .....	5
Threshold Calculation .....	9
DETECTOR CHARACTERISTICS .....	9
Probability of False Alarm vs Threshold .....	11
Threshold Estimate .....	11
Detector Operating Characteristics .....	14
Position Estimation .....	14
Discussion of Results .....	17
SUMMARY .....	18
REFERENCES .....	18
APPENDIX A—Importance Sampling .....	19



## A DETECTOR DESIGN FOR THE SPS-10 RADAR

### INTRODUCTION

A system that merges target reports from several naval radars into a single track file (sensor integration) is currently being developed by the Naval Research Laboratory (NRL) and is reported in NRL Report 7678 [1]. This previous report describes the basic system philosophy and the automatic detectors for the SPS-12 and SPS-39 radars. The present report describes the design of an automatic detector for the SPS-10 radar, which is a part of the sensor integration program. The detector chosen exhibits good target detection sensitivity while maintaining a low probability of false alarm  $P_{fa}$ . In addition, the detector can be constructed at a reasonable cost.

The SPS-10 C-band radar has a  $0.25\text{-}\mu\text{s}$  pulse and a  $1.5^\circ$  beamwidth but has no sub-clutter visibility such as that provided by moving-target indicators (MTI). The PRF is 660 pps and the scan rate is 15 rpm. This radar is primarily used for surface search aboard naval ships, a fact that requires the detector to detect ships in sea clutter and in a noise-limited environment. The noise-limited case occurs at shallow grazing angles and at ranges beyond the radar horizon when the target's mast is within the line of sight of the radar.

### DETECTOR SELECTION

Detectors can be classified into two basic categories: nonparametric and parametric. The nonparametric detectors maintain a constant false alarm rate (CFAR) for any noise distribution while ideally suffering only a small loss in detection sensitivity. Parametric detectors are optimum detectors for a known noise distribution but may suffer a large sensitivity loss for varying noise distributions.

#### Nonparametric Detectors

Since the SPS-10 radar is basically operating in a clutter environment and has false-alarm problems, it would appear that nonparametric detectors would be ideal. Unfortunately, this is not the case. C-band doppler spectra of sea clutter [2] show that decorrelation time varies from about 40 ms at sea state 2 to about 10 ms at sea state 7. Thus, since the time on target is only 17 ms, only one, two, or three of the 11 pulses on target can be assumed to be independent. Consequently, the behavior of a nonparametric detector with the 11 dependent samples is bounded by the behavior of the nonparametric detector with three independent samples. Unfortunately, the sensitivity loss associated with a nonparametric detector which uses only a few independent samples is very large. For instance, the losses associated with the Kendall tau [3], Spearman rho [3], and generalized sign test [4] are greater than 8 dB when only three independent samples are

---

Note: Manuscript submitted February 7, 1974.

available. Therefore, because of this large sensitivity loss, nonparametric detectors will not be used.

### Parametric Detectors

When the received signal is composed of a known signal and additive white Gaussian noise, the optimal noncoherent detector is closely approximated by a weighted sum of envelope-detected pulses whose weights are proportional to the signal-to-noise ( $S/N$ ) ratio. In turn, this detector is closely approximated (within 0.15 dB) by a 2-pole filter [5] which is the video integrator that will be used with the SPS-10.

A low false alarm rate is obtained by using a cell-averaging CFAR to estimate the mean of the signal. If the samples were independent and Rayleigh distributed, this single estimate would provide CFAR. However, the clutter samples are not independent and may not be always Rayleigh distributed. Therefore, the surrounding cells are used to estimate the standard deviation of the noise. Specifically, the mean deviate estimate\* is used because of implementation considerations.

However, if the decorrelation of the noise changes, the distribution of the integrated output will also change;† and consequently, a CFAR will not be maintained. Of course, if the detector is designed with the assumption that only a few samples are independent, a low false alarm rate will result. The adjustment of the threshold is detailed later in the Detector Characteristics discussion.

## DETECTOR IMPLEMENTATION

The basic elements of the proposed detector for the SPS-10 radar are shown in Fig. 1. The analog-to-digital (A-D) convertor operates at a rate of one over the pulse width. Therefore, on a given range sweep of the radar, the video is quantized into a number of range cells. The 2-pole video integrator integrates the sweep-to-sweep radar returns in each range cell. Shift registers (SR) are used for storage elements. A target is declared in a given range cell if its signal level is above an adaptive threshold. The threshold is calculated by estimating the mean and standard deviation of the noise in nearby range cells and setting the threshold a fixed number of standard deviations above the mean value. Each circuit element will next be described in detail.

### Analog-to-Digital Converter

The A-D converter operates at a rate of one over the pulse width, i.e., 4 MHz. The dynamic range of the SPS-10 receiver is 50 dB. However, a 10-bit A-D converter is required yielding a 60-dB dynamic range. The reason for this is that the last few bits of the converter must be noisy under thermal noise input conditions so that a reasonable estimate of the standard deviation can be made for setting the threshold. If the quantization was quite coarse, the standard deviation could be zero, yielding a wrong estimate of the threshold.

\*See definition, Eq. (10).

†This is due to the few number of independent samples. If there were many independent samples, the output would be Gaussian by the central limit theorem.



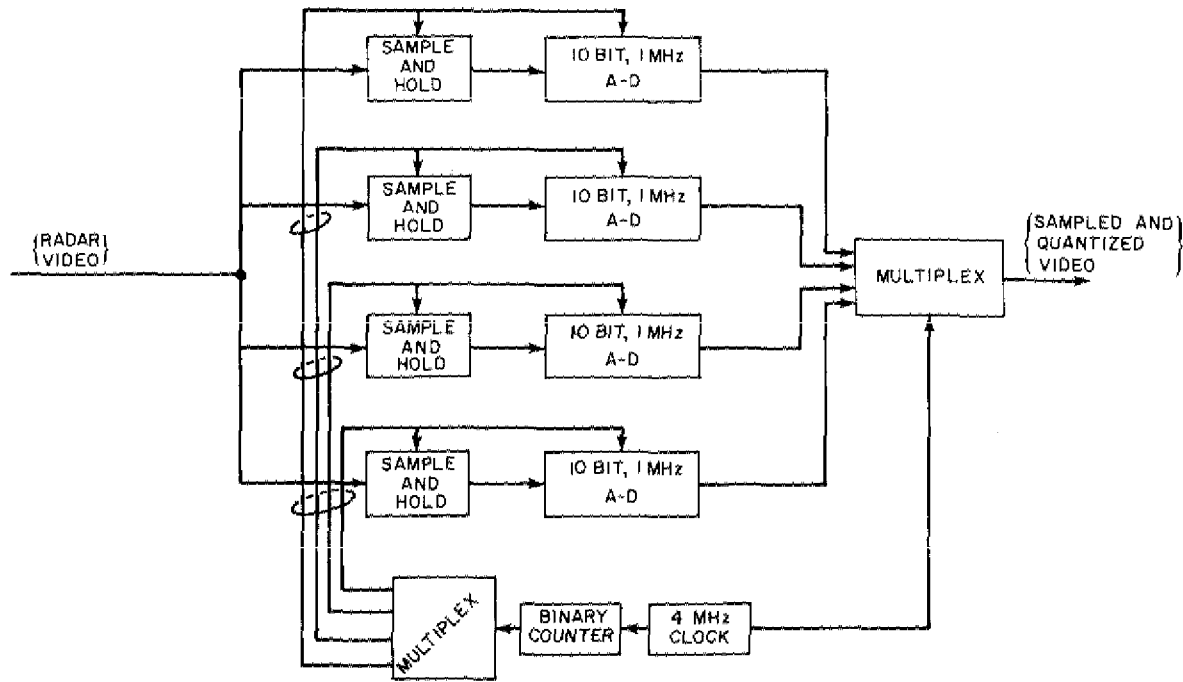


Fig. 2 - A practical 4-MHz, 10-bit A-D converter

The maximum steady state values the filter can obtain are

$$\text{Max } \{y_2(i)\} = \frac{\{\text{Max } x(i)\}}{(1 - k_1 + k_2)} \quad (6)$$

$$\text{Max } \{y_1(i)\} = (k_1 - 1) \text{Max } \{y_2(i)\}. \quad (7)$$

The maximum value of  $x(i)$  is 1024 which is the maximum value available from the 10-bit A-D convertor. If the input is guaranteed to be always large enough,  $y_1(i)$  and  $y_2(i)$  will always be positive and therefore a sign bit is not required in the filter. Consequently, 256 is added to the input  $x(i)$ ; and this guarantees that no negative numbers appear in the filter, if it is correctly initialized. Therefore,

$$\text{Max } \{y_2(i)\} = 16 (1024 + 256) \quad (8)$$

$$\text{Max } \{y_1(i)\} = 10 (1024 + 256). \quad (9)$$

Thus, 15 bits are sufficient to accommodate the largest steady state number possible and the transient overshoot.

The outputs of the multipliers and summers must be rounded off. By simulation it was found that the round-off error was sufficiently small if two bits below the decimal point were used. Therefore the total number of bits required in each word of the shift registers is 17.

The number of words required in the shift registers is set by the desired instrumented range and the range resolution. We choose the shift registers to be 2048 words long, which corresponds to a range of 41.4 nm using the 0.25- $\mu$ s pulse mode. The 2-pole filter design is shown in Fig. 3. Before the filter is placed in operation, the initial conditions are shifted into all word locations of the shift register by closing the normally open NO switches and opening the normally closed NC switches. The two multipliers are not ordinary serial multipliers. The multiplication is performed by using two summers and properly shifting the multiplicand. When the filter is operating in this manner, three serial adds must be performed in 0.25  $\mu$ s, and the required 80 ns per add is feasible in today's hardware.

#### Estimates of Mean and Standard Deviation

The threshold is calculated from the estimates of the mean and standard deviation using the range cells surrounding the test cell. If too many range cells are used, the estimate will not represent the environment near the test cell. If too few are used, the estimates will have a large variance. The number of range cells on each side of the test cell was chosen to be 16. Furthermore, since ships can be as long as 1000 ft, an additional 6 cells on each side of the test cell will not be used, so that the target is not included in the noise estimates. The shift register configuration is shown in Fig. 4. The total length of the shift registers in range is about 1 n.mi.

CANTRELL, TRUNK AND QUEEN

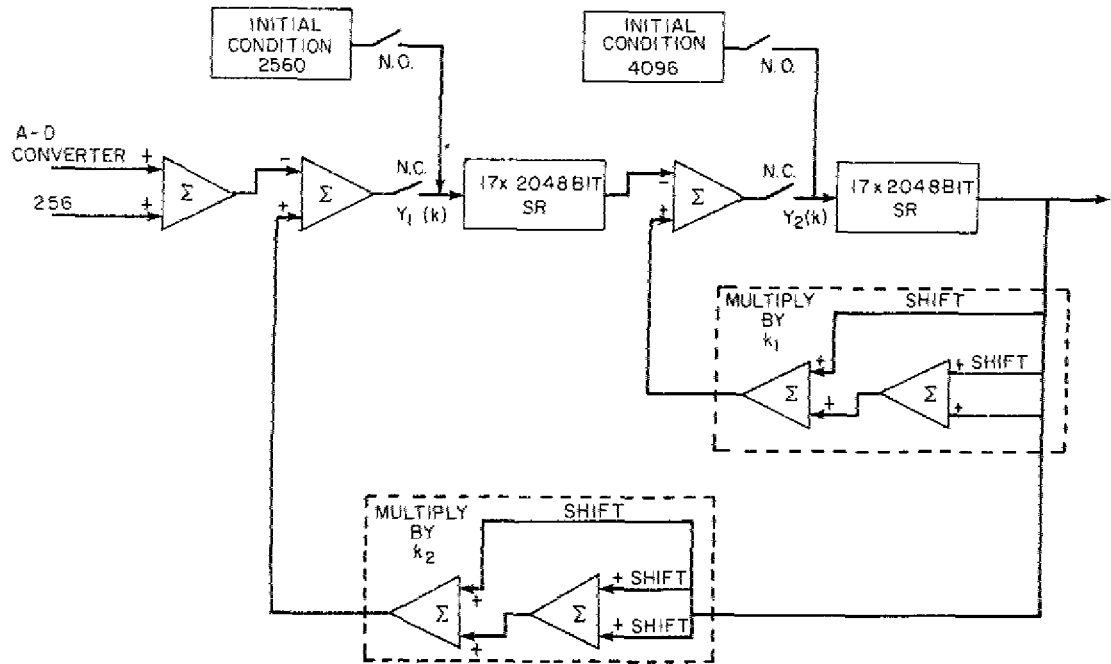


Fig. 3 — Two-pole filter used as a video integrator

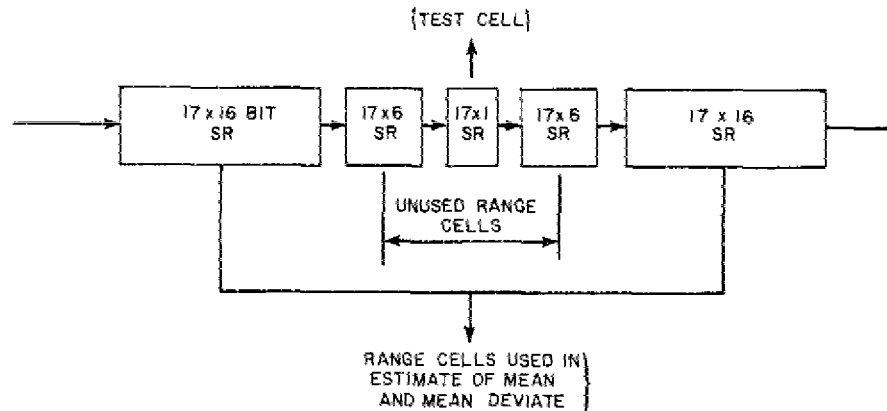


Fig. 4 — Shift register configuration for adaptive threshold

The mean value  $\mu$  is calculated by performing a running average as shown in Fig. 5. Assume that the sum  $S$  at the output of the sum register is correct at a given clock pulse. On the next clock pulse, the new values entering the 16-word shift registers are added to the sum  $S$  and the old values leaving the registers are subtracted, thus yielding the correct sum on the new clock pulse. The circuit is initialized by opening the NC and closing the NO switches after the instrumented range has been processed. The values at the output of the adders will always be positive and therefore there is no need for complementation. The division by 32 is achieved by redefining the binary point. The mean value is delayed one clock pulse from the values which were used to compute it. The first and last 19 range cells of the instrumented range can not be used because the mean value will yield the wrong results in these regions.

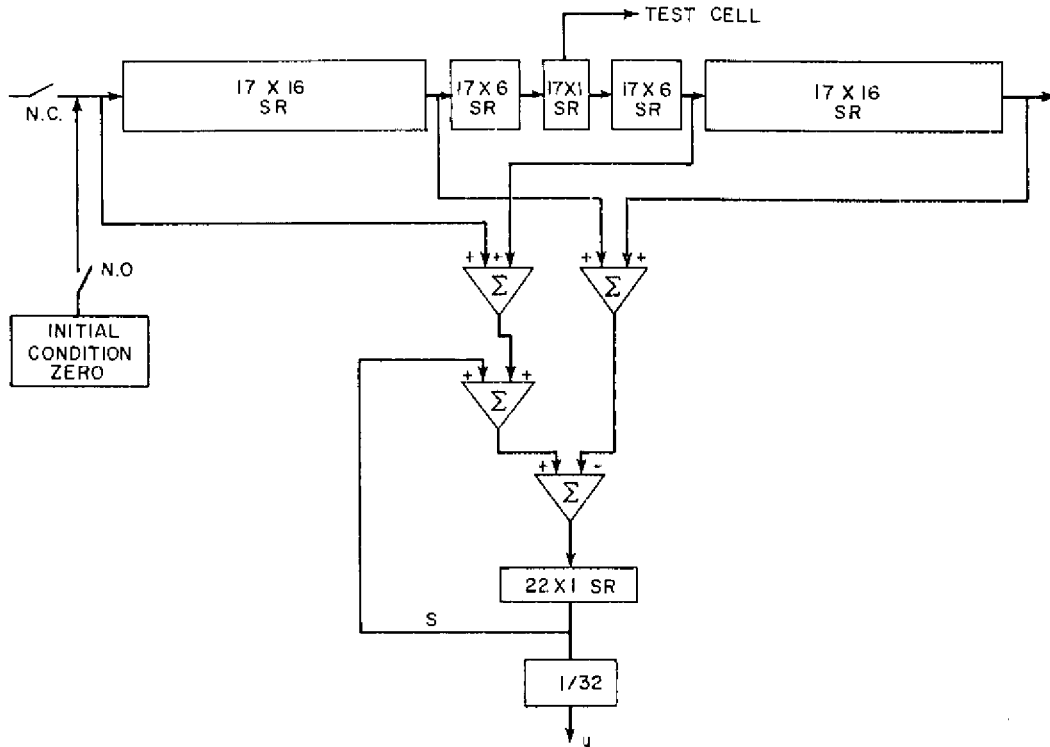


Fig. 5 - Circuit for computing the mean

After the mean has been estimated, the standard deviation is estimated using the mean deviate estimate; i.e.\*

$$\sigma = \frac{B}{32} \sum_{L=1}^{32} |y_i - \mu| \tag{10}$$

where  $\{y_i\}$  = the values in the surrounding 32 cells

$$\mu = \frac{1}{32} \sum_{L=1}^{32} y_i \tag{11}$$

Because so many calculations are involved in Eq. (10), they will be performed in hardware over several clock pulses. As mentioned previously,  $\mu$  is calculated on the first clock pulse. After  $\mu$  is available, each of the terms  $|y_i - \mu|$  is computed, Fig. 6, by subtracting  $\mu$  from each of the 32 cells, forming the absolute value, and storing the results in registers at the next clock pulse. The summation in Eq. (10) is shown in Fig. 7. The summation is performed over two clock periods with the intermediate results being stored in registers. The division by 32 is just a shift in the decimal point.

\*The constant  $B$  equals  $\sqrt{\pi/2 \cdot 32/31}$ . If the mean is known a priori the constant  $B$  equals  $\sqrt{\pi/2}$ .

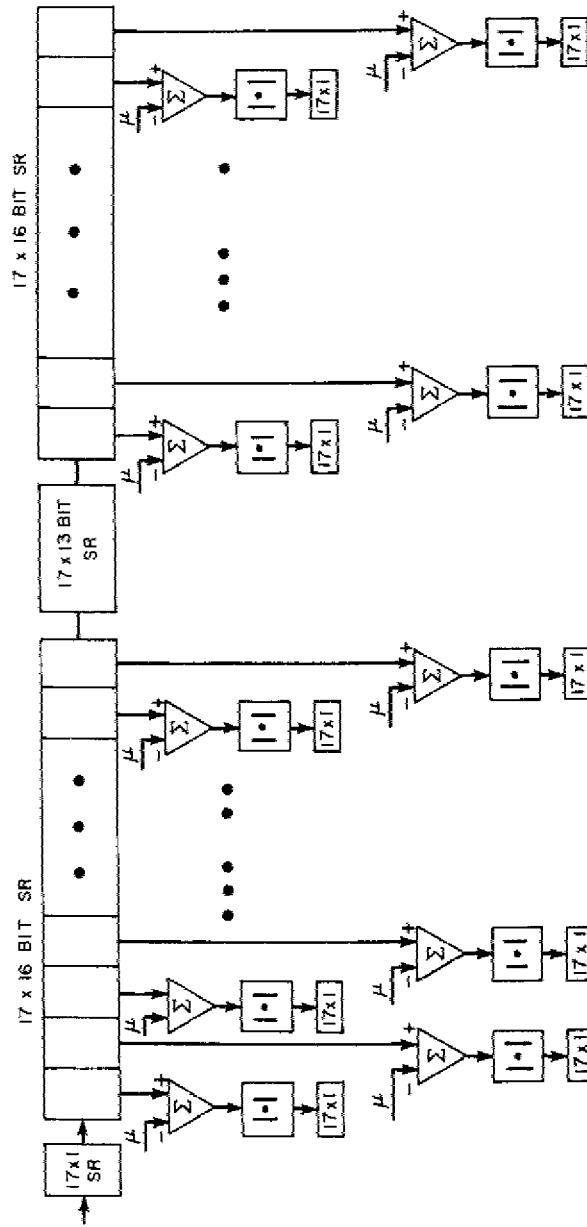


Fig. 6 — Circuit for calculating each term in the sum when the mean deviate is being computed

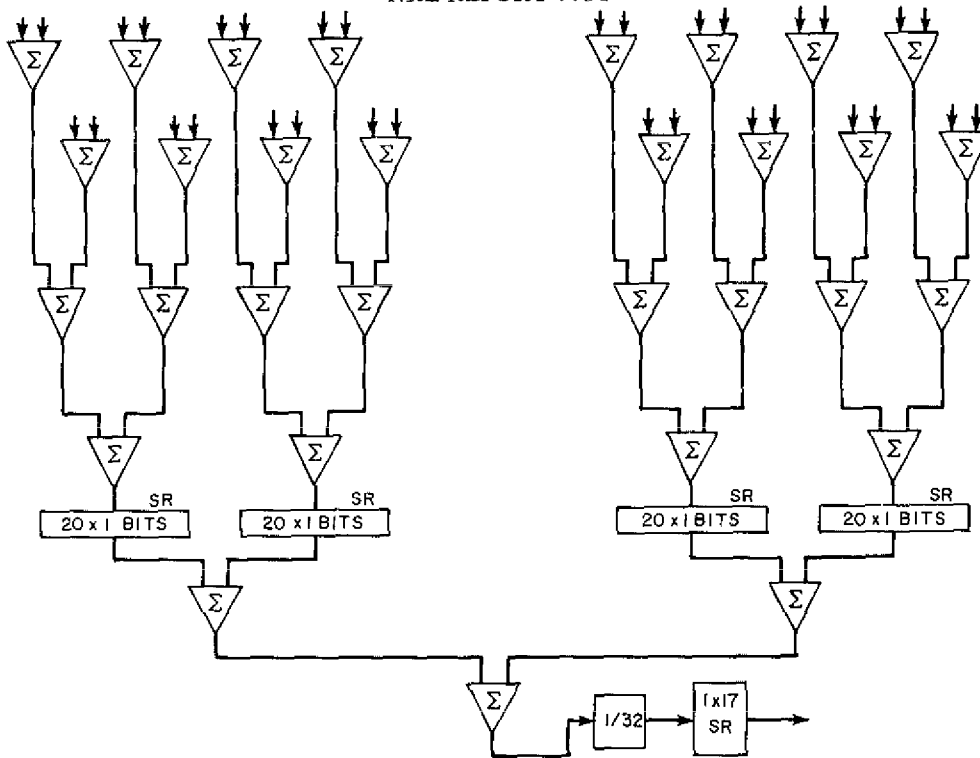


Fig. 7 - The summation of the term when the mean deviate is being computed

**Threshold Calculation**

The threshold is given by

$$T = \mu + \frac{K}{32} \sum_{L=i}^{32} |y_i - \mu| = u + K\sigma_d \tag{12}$$

and the circuitry is shown in Fig. 8. The number  $K$  is represented by 11 bits,  $K(1)$ ,  $K(2)$ , ...,  $K(11)$ . The multiplication by  $K$  is performed by a number of shifts and additions, the shifts being hardwired. The additions are performed in two clock pulses. The mean, which was computed 4 clock pulses earlier, is then added to form the threshold  $T$ .

The detection is made by comparing the test range cell against the threshold as shown in Fig. 9. Since it took 6 clock pulses to obtain the threshold, the test cell must be delayed by 6 pulses.

**DETECTOR CHARACTERISTICS**

In this section, the questions how well the detector will perform and what value should be assigned to  $K$  are investigated. We begin by computing the thresholds required to achieve a given probability of false alarm  $P_{fa}$ . The effects of estimating the threshold are outlined and the value of  $K$  is set. Then, the operating characteristic of the detector

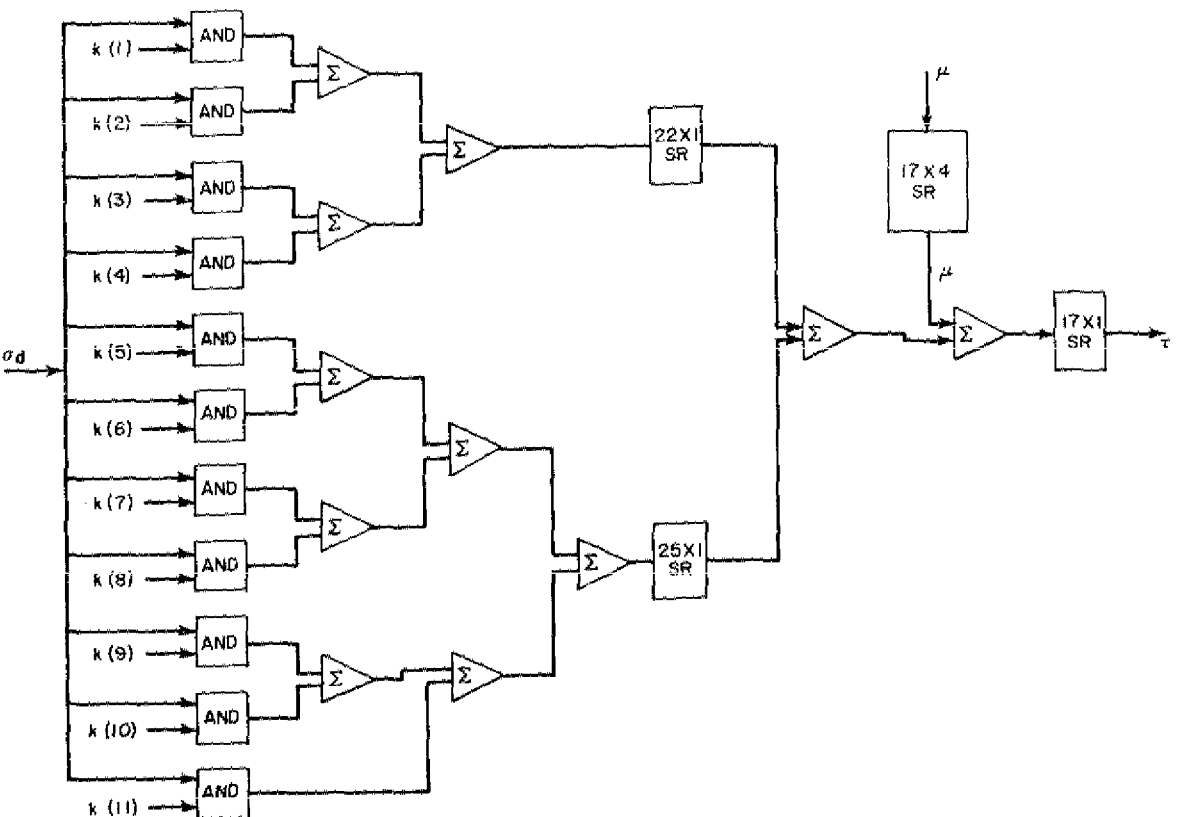


Fig. 8 — Circuit for computing the threshold  $T = \mu + K\sigma_d$

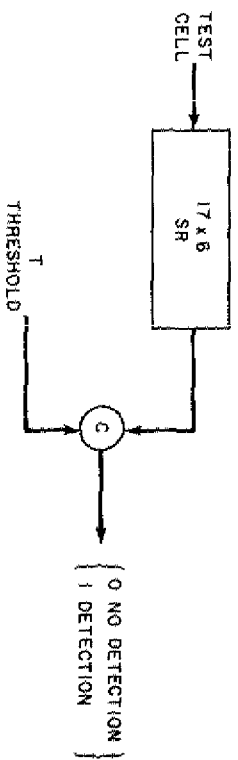


Fig. 9 — Threshold comparison for detection

(probability of detection  $P_D$  vs  $S/N$  for a fixed  $P_{fa}$ ) is calculated. Finally, the method of estimating the target position is detailed.

### Probability of False Alarm vs Threshold

The  $P_{fa}$  for a given threshold is found by the simulation shown in Fig. 10. The distribution of sea clutter is essentially Gaussian [6] in both the  $I$  and  $Q$  channels. However, the Gaussian noise is correlated. To simulate correlated Gaussian noise, an independent Gaussian noise source is passed through a low-pass filter. The low-pass filter chosen is described by Eq. (1), and the coefficients are given by Eqs. (2) and (3). The normalized correlation property of the filter is shown in Fig. 11 for three different sets of filter coefficients, in which  $n_p$  is approximately the number of pulses correlated and defined as the value of  $N$  in Eqs. (2) and (3). The case of  $n_p = 0$  corresponds to white or thermal noise and is obtained by setting  $k_1$  and  $k_2$  to zero. The standard deviation at the output of the filter in terms of the standard deviation of the independent Gaussian noise source is

$$\sigma_0 = \frac{\sigma}{\sqrt{1 - k_1^2 - k_2^2 + \frac{2k_1^2 k_2}{1 + k_2}}} \quad (13)$$

Therefore, the output of the low-pass filter must be multiplied by

$$\sqrt{1 - k_1^2 - k_2^2 + \frac{2k_1^2 k_2}{1 + k_2}} \quad (14)$$

so that the power level is the same for all  $n_p$ 's at the output of the noise source. The simulation is completed by finding the signal envelope and passing this through the video integrator as previously described.

The straightforward way of computing the  $P_{fa}$  for a number of threshold settings is to repeat the simulation many times and thus estimate the distribution of  $y$ . However, obtaining the tail of the distribution, requires a very large number of trials when this method is used. A method of obtaining the tails using a small number of trials is called importance sampling [7]. This technique is described in the appendix and the results of the technique are given in Fig. 12. It is found that the threshold must be higher, if the noise is correlated, in order to achieve a given  $P_{fa}$ . The reason for this is that the variance is higher because there is less relative smoothing in the filter for the correlated noise cases. It is interesting to note that the  $n_p = 0$  case is closely approximated by a Gaussian distribution of the same mean and variance.

### Threshold Estimate

In the preceding section, the  $P_{fa}$  vs  $T$  was calculated. However, since  $T$  is estimated using Eq. (12), the entire system, Fig. 1, is simulated under noise only conditions. The mean and standard deviations of the noise estimates, based on 32 samples, are computed

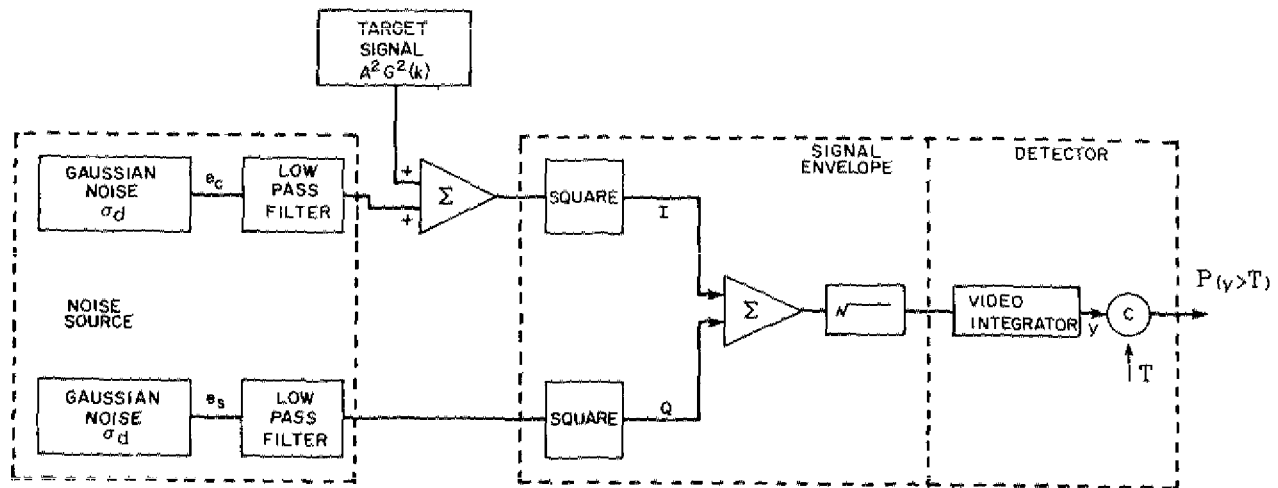


Fig. 10 — Simulation used in obtaining the detector characteristics

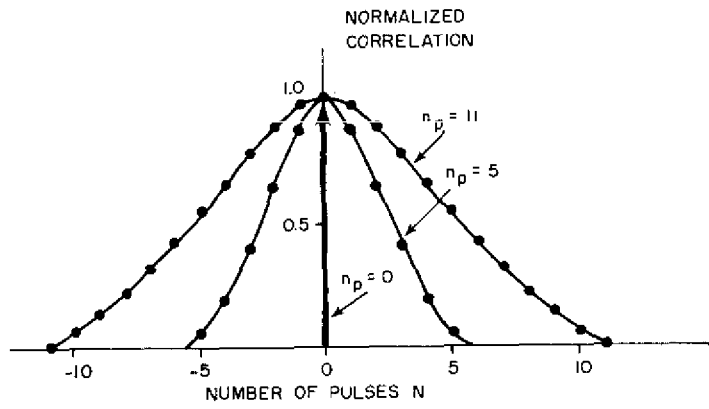


Fig. 11 — Correlation property of the noise at the output of the low-pass filter

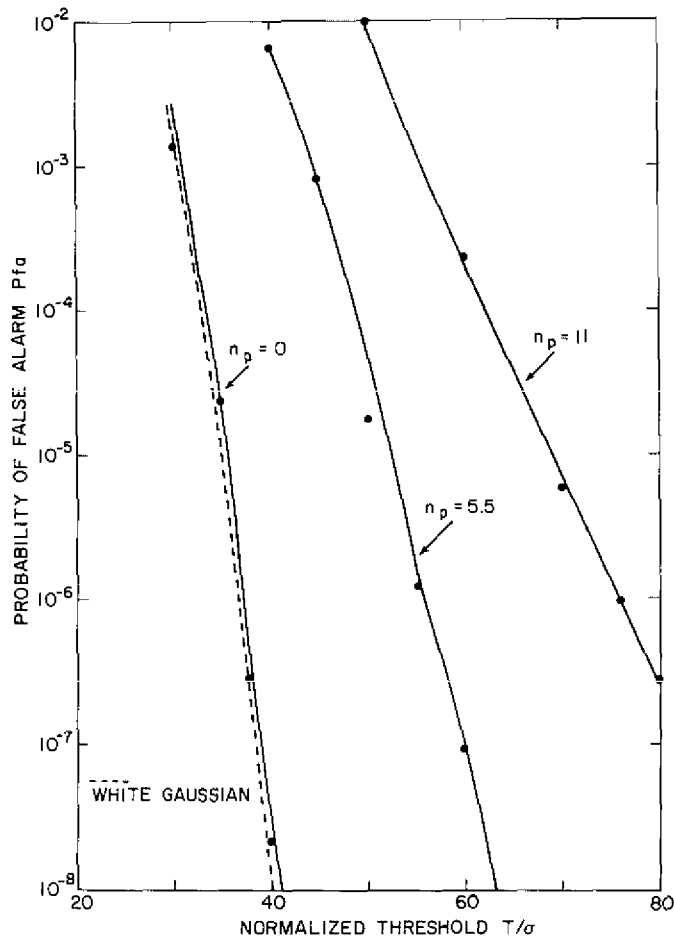


Fig. 12 — Probability of false alarm for various noise correlations as a function of the normalized threshold

Table 1  
Mean and Variance of Estimate of The True Mean  $\mu$  and Mean Deviate  $\sigma_d$

Correlation $n_p$	$\bar{u}$	$\sigma_u$	$\sigma_d$	$\sigma_{\sigma_d}$
0	19.22	0.66	2.99	0.41
5.5	19.86	1.13	5.01	0.73
11	19.91	1.46	6.53	1.00

and the results are shown in Table 1. With the use of Table 1, Fig. 11, and the formula  $\bar{T} = \bar{\mu} + K\bar{\sigma}_d$ , the value of  $K$  that yields  $P_{fa} = 10^{-6}$  can be computed. The results for  $n_p = 0, 5.5, \text{ and } 11$  are  $K = 5.95, 7.36, \text{ and } 8.74$ , respectively. Thus, no one value of  $K$  will yield CFAR. This is because the distribution of the output of the 2-pole filter is different for various amounts of correlation.

The value of  $K$  was chosen to be 7.36. The  $P_{fa}$  for various correlations is given by

$$P_{fa} = \int_0^{\infty} P(T)P_{fa}(T)dT, \quad (15)$$

where  $P_{fa}(T)$  is given in Fig. 12 and the density of  $T$  is Gaussian with its mean given by  $\bar{\mu} + K\bar{\sigma}_d$  and its variance given by  $\sigma_u^2 + K^2\sigma_{\sigma_d}^2$ . Performing a numerical integration of Eq. (15) yields  $P_{fa} = 5 \times 10^{-7}, 3 \times 10^{-5}, \text{ and } 2 \times 10^{-4}$  for  $n_p = 0, 5.5, \text{ and } 11$ , respectively.

#### Detector Operating Characteristics

The  $P_D$  vs  $S/N$  for a given  $P_{fa}$  is found by the simulation described in Fig. 10. The target signal is  $A^2G^2(i)$  where  $G(i)$  is the  $(\sin x)/x$  antenna pattern containing 11 pulses within the 3-dB beamwidth. If we let the standard deviation of the Gaussian noise sources be one,  $S/N = A^2/2$ . The simulation is repeated many times and  $P_D$  is calculated by

$$P_D = \frac{\text{Number of times } y \text{ exceeds } T}{\text{Total number of trials}}, \quad (16)$$

where  $T$  is set by Eq. (12) with  $K = 7.36$ . The detection results are shown in Fig. 13. We see that  $P_D$  is lower for correlated noise. The reason for this is the higher threshold required for correlated noise.

#### Position Estimation

After a target has been detected its position must be estimated. Because of the high range resolution of the SPS-10 radar, a single ship may be detected in more than one range cell. This situation causes an ambiguity in that several detections in nearby range

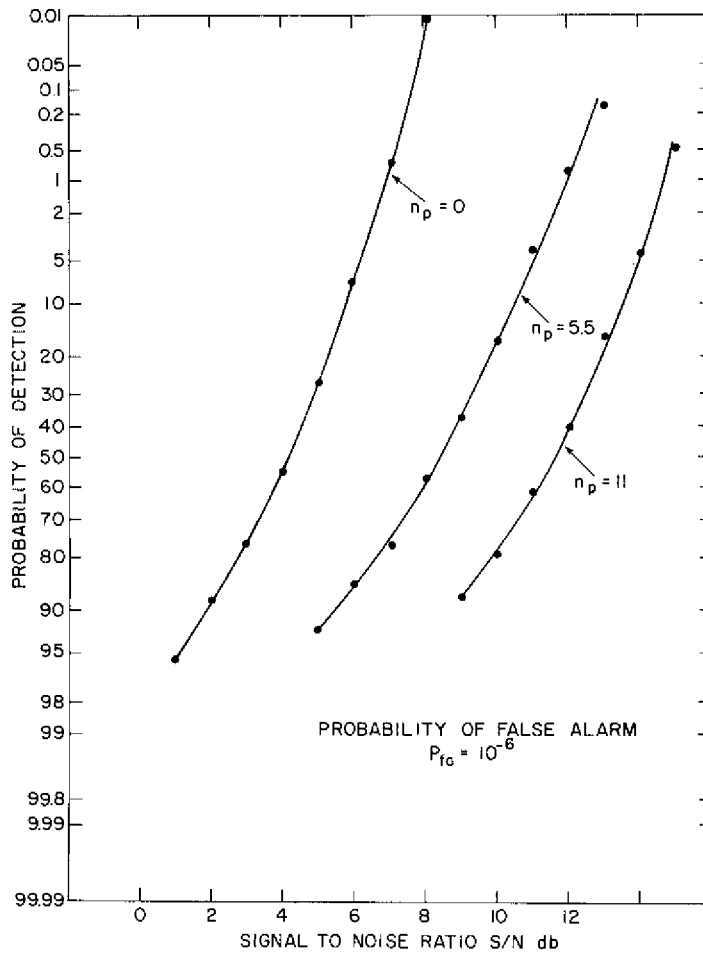


Fig. 13 — Detector operating characteristics

cells can be considered either several small targets or one large target. Observing this fact, we can conclude that the range resolution of the radar is no better than the largest target under consideration unless further information is provided so that the ambiguity can be resolved. This does not mean the high resolution radar should not be used. The detection capability in clutter is improved for small targets and for large targets which have only a few dominant scattering surfaces. We now consider the estimates of the target position.

The largest ship we expect to see is 8 range cells long. This determines the range resolution of the measurement since no other information is available. Therefore, the detections over all 8 range cells are merged as shown in Fig. 14. For a single range extended target, the merged detections either look like a single target or two targets because of range gate splitting and because the range resolution of the measurement is 1000 ft rather than 125 ft.

The implementation of the azimuth measurement is shown in Fig. 15. Merged radar detections (1 = a target or 0 = no target) are first gated. If a target has been detected in the preceding range cell on the  $i$ th pulse or the following range cell on the  $(i - 1)$ th pulse,

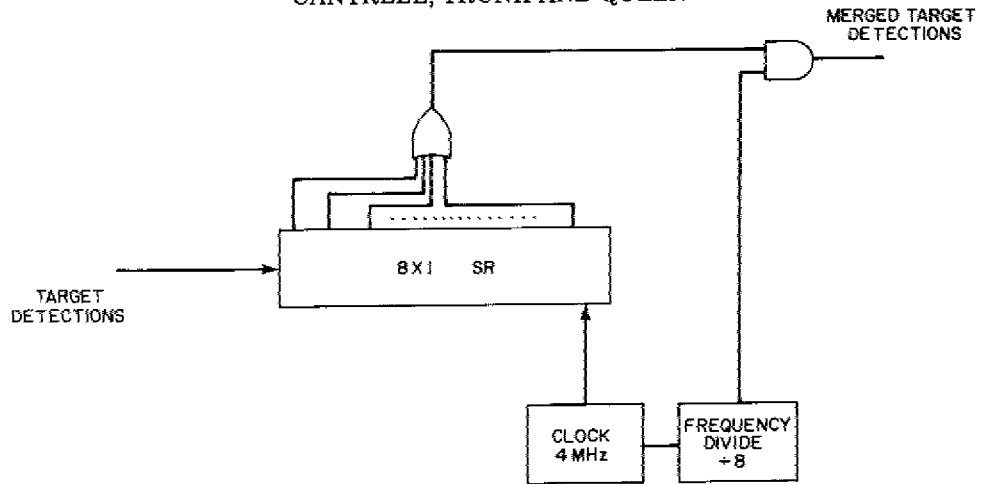


Fig. 14 — Circuit for merging every eight range cells

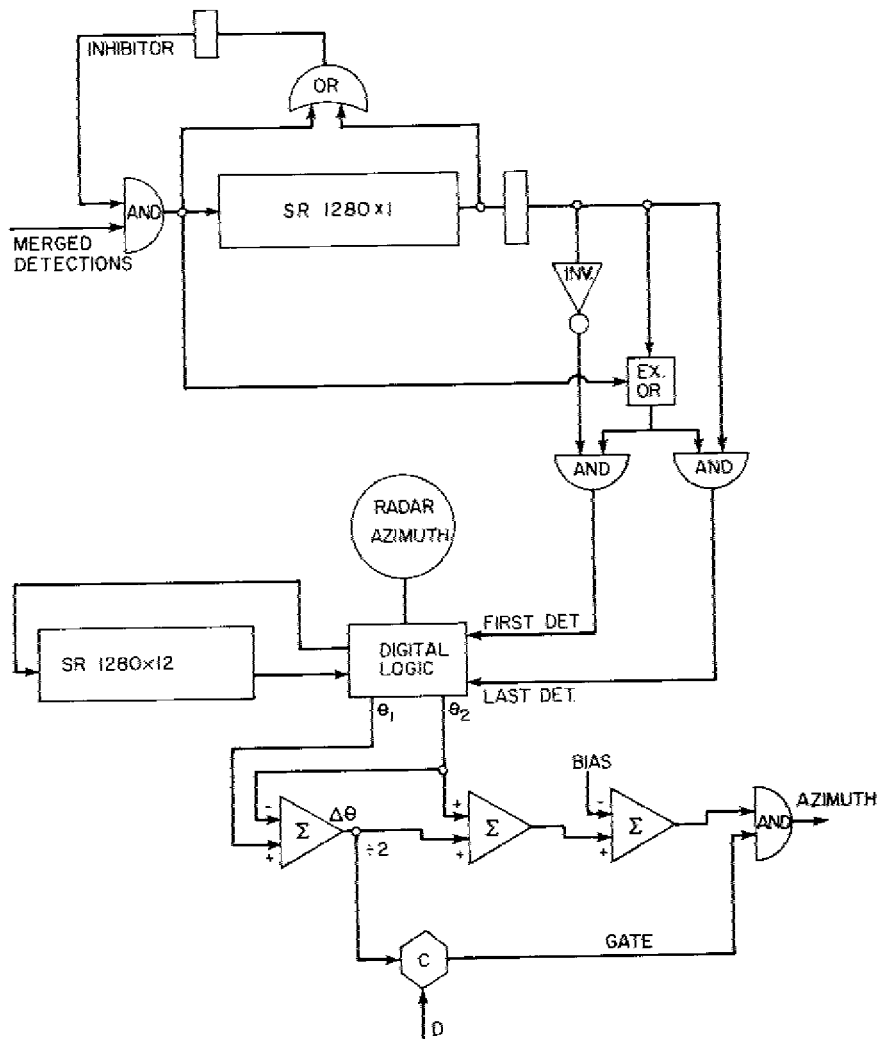


Fig. 15 — Circuit for estimating angular position

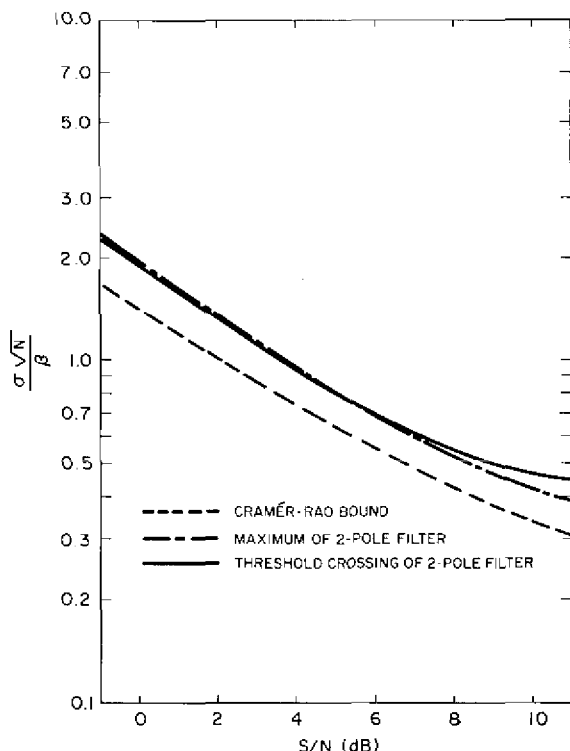


Fig. 16 — Comparisons of angular estimates with the Cramer-Rao lower bound.  $\sigma$  is the standard deviation of the estimation error and  $N$  is the number of pulses with the 3-dB beamwidth, which is  $2\beta$ . (From B.H. Cantrell and G. V. Trunk, *IEEE Trans. AES-9*, p. 652 (1973).)

the detection is inhibited. This logic eliminates a target being detected in adjacent range cells. The gated input on the  $i$ th pulse is then compared, with an exclusive OR, to the  $(i - 1)$ th pulse. Two AND circuits are used to identify the initial detection 10 and final detection 01. At the first detection, the radar azimuth is read into a shift register. This circulates in the shift register until the last detection. At this time both azimuth positions are averaged and the bias value is subtracted to yield the azimuth estimate. By using modulo arithmetic and the one's complement in the subtraction, the discontinuity in the zero point problem is circumvented. If the azimuth extent of the target is too long, the detection is inhibited.

The accuracy of the azimuth estimate is a function of signal-to-noise ratio, and the result is shown in Fig. 16 [5].  $N$  is the number of pulses,  $2\beta$  is the 3-dB beamwidth, and  $\sigma$  is the standard deviation of the azimuth error. The bias of the estimate varies from  $1.0\beta$  to  $1.1\beta$  as a function of signal to noise ratio [5], a fixed bias of  $1.575^\circ$  is used.

### Discussion of Results

In the preceding section it was shown that the detection capability of the detector decreases as the noise became more correlated. It was also shown that, if one places the

threshold  $K$  mean deviates above the mean, the  $P_{fa}$  can not be held constant. This was true because the distribution at the video integrator output would change form as a function of the correlation. In addition, the threshold was estimated using 32 random samples and therefore was a random variable. The combined effects of the correlation and the finite sample size would make the  $P_{fa}$  vary from about  $10^{-4}$  to  $10^{-7}$ , with a  $K$  of 7.36. However, we feel that a detector of the type described will yield an acceptable false alarm rate, obtain a reasonably good probability of detection, and make an accurate position estimate.

In the discussion in this section, homogeneity in the 32 sample cells has been assumed. This is not always true; for example, a part of the cells may represent land clutter and the remaining ones thermal noise; or else, there may be other targets in the 32 cells. The effect of these conditions is to raise the threshold, and the detector's sensitivity is drastically reduced. There are circuits for improving this situation, but they were not used because of the extra cost. Also, the value of  $K$  was assumed to be constant. This value probably will be made adaptive with respect to sectors swept by the radar by monitoring the number of hits in these radar sectors and adjusting the threshold accordingly.

### SUMMARY

A detector for the SPS-10 radar that uses a video integrator and adaptive threshold was described. The circuits were designed in sufficient detail to ensure their operation with present-day hardware. The detector, although not ideal, was shown to yield a reasonable false alarm rate and to obtain reasonable detection results.

### REFERENCES

1. G. Trunk, B. Cantrell, and D. Queen, "Sensor Integration: Basic System Concept and Automatic Detection," NRL Report 7678, Mar. 7, 1974.
2. G.R. Valenzuela and M.B. Laing, "Study of Doppler Spectra of Radar Sea-Echo," NRL Report 6934, Nov. 3, 1969.
3. V.G. Hansen, "Detection Performance of Some Nonparametric Rank Tests and an Application to Radar," IEEE Trans. IT-16 (No. 3), 309-318 (May 1970).
4. V.G. Hansen and B.A. Olsen, "Nonparametric Radar Extraction using a Generalized Sign Test," IEEE Trans. AES-7 (No. 5), 942-950 (1971).
5. B.H. Cantrell and G.V. Trunk, "Angular Accuracy of a Scanning Radar Employing a 2-Pole Filter," IEEE Trans. AES-9 (No. 5), 649-653 (1973).
6. G.V. Trunk, "Radar Properties of Non-Rayleigh Sea Clutter," IEEE Trans. AES-8 (No. 2), 196-204 (1972).
7. F.S. Hillier and G.J. Lieberman, *Introduction to Operations Research*, Holden-Day, Inc., 1967, 457-459.

## Appendix IMPORTANCE SAMPLING

The fundamental principle of the technique of importance sampling is to modify the probabilities that govern the outcome of the basic experiment of the simulation in such a way that the event of interest (i.e., the false alarm) occurs more frequently. This distortion is then compensated for by weighting each event by the ratio of the probability that this specific event would have occurred if the true probabilities had been used in the simulation to the probability that this same event would occur with the distorted probabilities. Consequently, by proper choice of the distorted probabilities the number of repetitions can be reduced greatly.

To illustrate the method, we operate the simulation shown in Fig. 10 over 20 pulses and then reset using the last values as the initial values for the next run of 20 pulses. Now to obtain more events on the tail of the distribution, the original probabilities are distorted so that more events occur on the tail. This is achieved by making the variance of the white Gaussian noise generators larger. The simulation is run and the probability density of  $y$  is computed by

$$P(y \text{ is in } nth \text{ interval}) = \frac{1}{M} \sum_{j=1}^M S_j$$

where

$$S_j = \begin{cases} \prod_{i=1}^{20} \frac{P_T(e_c(i))P_T(e_s(i))}{P_D(e_c(i))P_D(e_s(i))} & Z \text{ lays in} \\ & nth \text{ interval} \\ 0 & Z \text{ is out of} \\ & nth \text{ interval} \end{cases}$$

$e_c(\cdot)$  and  $e_s(\cdot)$  are the  $I$  and  $Q$  Gaussian noise components, and  $P_T(\cdot)$  and  $P_D(\cdot)$  are the true and distorted probability densities, respectively, evaluated at the values the noise sequence takes on. Because both  $P_T(\cdot)$  and  $P_D(\cdot)$  are Gaussian

$$S_j = \prod_{i=1}^{20} \frac{\sigma_D^2}{\sigma_T^2} \exp \left[ \frac{e_c^2(i)}{2} \left( \frac{1}{\sigma_D^2} - \frac{1}{\sigma_T^2} \right) - \frac{e_s^2(i)}{2} \left( \frac{1}{\sigma_D^2} - \frac{1}{\sigma_T^2} \right) \right]$$